# Lattice dynamics and migration enthalpies in $CoPt_3$ and FePd

T. Mehaddene,[1,*] E. Kentzinger,[2,3] B. Hennion,[4] K. Tanaka,[5] H. Numakura,[6] A. Marty,[7] V. Parasote,[3] M. C. Cadeville,[3] M. Zemirli,[1] and V. Pierron-Bohnes[3]

[1]*LPCQ, University M. Mammeri, 15000 Tizi-Ouzou, Algeria*

[2]*Institut für Festkörperforschung, Forschungszentrum Jülich, D-52425 Jülich, Germany*

[3]*IPCMS, CNRS-ULP, 23 rue du Loess, Boîte Postale 43, F-67034 Strasbourg Cedex 2, France*

[4]*LLB, CEA Saclay, F-91191 Gif sur Yvette Cedex, France*

[5]*Department of Advanced Materials Science, Kagawa University, Takamatsu 761-0396, Japan*

[6]*Department of Materials Science and Engineering, Kyoto University, Sakyo-ku, Kyoto 606-8501, Japan*

[7]*SPMM/DRFMC/CEA, 17 avenue des martyrs, F-38054 Grenoble Cedex 09, France*

(Received 15 June 2003; revised manuscript received 19 September 2003; published 23 January 2004)

The frequencies of the normal modes of vibration of $CoPt_3$ and FePd single crystals have been measured using inelastic neutron scattering. The measurements were performed in the $L1_2$ ordered phase (at 300 and 930 K) for $CoPt_3$ and in the $L1_0$ ordered phase (at 300 and 860 K) for FePd. Dispersion curves were also measured in the fcc disordered states, at 1060 and 1020 K for $CoPt_3$ and FePd, respectively. The activation enthalpy of atomic migration has been evaluated from the phonon density of states by applying Schober's model [H. R. Schober *et al.*, J. Phys.: Condens. Matter **4**, 9321 (1992)] and its extension to the $L1_2$ ordered structure. The phonon properties of $FePd_3$ reported in the literature have been analyzed similarly and are compared with the results for $CoPt_3$ and FePd. The contribution of the long-range order to the migration enthalpy estimated in the present analyses agrees well in magnitude with the previous evaluation by Monte Carlo simulation for alloys of the fcc, $L1_2$, and $L1_0$ structures.

DOI: 10.1103/PhysRevB.69.024304 PACS number(s): 63.20.−e, 78.70.Nx, 66.30.−h, 64.60.Cn

## I. INTRODUCTION

Intermetallics and ordered alloys form an important class of materials, and among them those presenting a phase diagram derived from the Au-Cu canonical phase diagram are of outstanding technological importance. After a period of extensive research on superalloys for their magnetic,[1–5] catalytic,[6] and high-temperature mechanical[7] properties, nowadays some of them in the systems of iron-group metals and platinum-group metals arouse new interests, owing to their possible applications as shape memory alloys[8,9] and high-density magnetic recording media because of their strong magnetic anisotropy.[10–12] Many properties of interest are linked to their ability to form ordered phases almost in coherence with the disordered matrix. A good knowledge of the ordering processes and of its dynamics is thus a necessary step in any extensive research on those systems. We have launched a systematic study of the physical, thermodynamic, and kinetic properties in the ordered alloys in the systems Fe-Pd, Fe-Pt, and Co-Pt. This paper reports the properties of phonons and the enthalpy of atomic migration in $CoPt_3$ and FePd.

Both systems are ferromagnetic at ambient temperatures, with the magnetic properties sensitive to the state of chemical order. For instance, the Curie temperature of the ordered $CoPt_3$ is 288 K, while it is 475 K if the alloy is quenched from the disordered state.[13] On the contrary, in FePd the Curie temperature is 763 K in the ordered state but is 673 K in the disordered state.[14,15] The chemical order-disorder transition ($T_C$) takes place in the temperature range 945–970 K and 920–965 K in $CoPt_3$ and FePd, respectively, at the stoichiometric composition, which in either case does not correspond to the congruent point.

The Co-Pt system has interested many researchers from a practical viewpoint as providing catalyst materials,[6] but from a basic viewpoint as a magnetic system with a coupling between chemical and magnetic ordering.[4,16] The $L1_2$ structure (also called the $Cu_3Au$ structure) has been observed at both $Co_3Pt$ and $CoPt_3$ compositions[13] (Fig. 1). In the $CoPt_3$ ordered structure, Pt atoms occupy the face centers and Co atoms occupy the cube corners (insert of Fig. 1). The $L1_0$ structure (also called the CuAu structure) has been observed on a wide concentration range between 44 and 56 at. % Pt. This ordered structure is based on the face-centered lattice of tetragonal symmetry and consists of alternating (001) planes of Co and Pt atoms (Fig. 2). It presents a tetragonal distortion of the lattice ($c/a<1$) and a uniaxial magnetic anisotropy. This system has been studied extensively to understand the origin of the asymmetry in its phase diagram. Various explanations have been proposed: for example, an effect of many-body interactions,[16] an influence of magnetism, and variations of atomic interaction with composition.[17,18] Calculation of this phase diagram may appear quite simple *a priori*, as it is based on the fcc lattice at almost all temperatures and compositions, but it still remains a challenge today. Nevertheless, reliable calculations have been made for the thermodynamic properties of the ordered phases by the cluster-variation method.[16] The theory predicts that the chemical long-range order (CLRO) of $CoPt_3$ would exhibit only a limited variation with temperature, namely, less than 10 % in the range from 300 K to 850 K, which is in agreement with the results of x-ray-diffraction[19] and nuclear-magnetic-resonance measurements.[20] The kinetics of atomic ordering in the ordered phases in this system has also been studied. The activation energy of changes in CLRO has been determined by

 

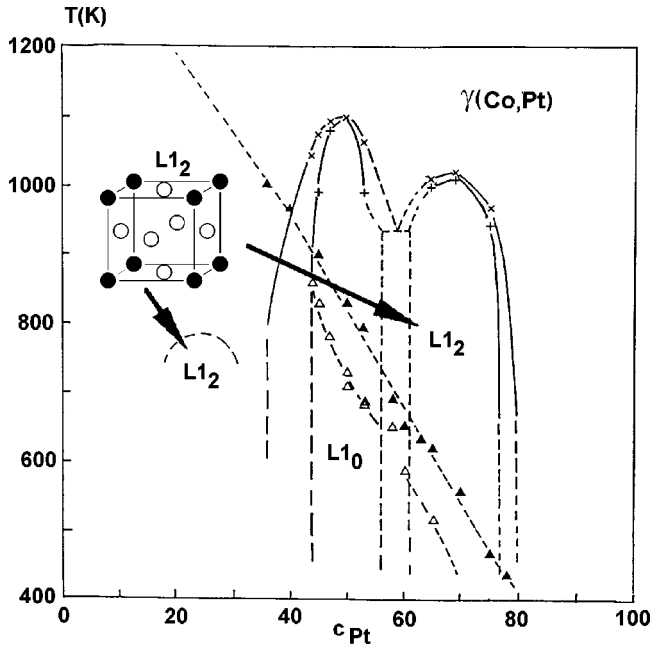


FIG. 1. Co-Pt phase diagram. The open and filled triangles show ferromagnetic ↔ paramagnetic transition temperature in the ordered and disordered states, respectively.

resistivity measurements to be 3.18 eV and 2.52 eV for $CoPt_3$ (Ref. 21) and CoPt,[22] respectively.

The Fe-Pd system has recently given rise to many studies as magnetic media[23,24] and shape memory candidate.[8] Earlier this system has attracted attention because of its Invar behavior around $Fe_3Pd$. Its phase diagram also presents the $L1_0$ and $L1_2$ ordered structures (Fig. 2) at low temperature in the ranges 0.48–0.60 and 0.60–0.80 at. %Pd, respectively.[25]

Among others, interesting behavior has recently been discovered on the variation of the CLRO with temperature. In an *in situ* high-temperature x-ray-diffraction experiment[26]

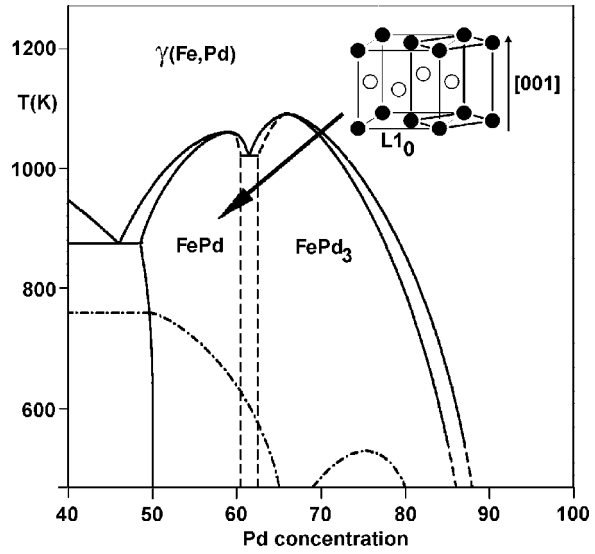


FIG. 2. A partial phase diagram of the Fe-Pd system. The dot-dashed curve indicates the ferromagnetic → paramagnetic transition temperature.

the relative intensities of the superlattice and fundamental diffraction peaks have been found to decrease significantly, roughly by a factor of 3, in the temperature range from 300 K to 860 K, which is far below the order-disorder transition temperature (920 K) but encompasses the magnetic Curie temperature (763 K), suggesting an influence of magnetic order on chemical order.

The kinetics of atomic ordering is quite rapid in this phase as shown by their possible use as shape memory alloys[8] as well as extensive studies recently started in this FePd phase. The kinetics of atomic ordering in FePd has been studied by resistivity measurements,[27,28] where two thermally activated processes have been found to be operative, similar to the case of the alloys in the Co-Pt system. The atomic mobility appears to be influenced by magnetism: the activation energy is higher in the ferromagnetic state than in the paramagnetic state. In connection to this, it is interesting to recall that a strong effect of magnetic ordering on the lattice dynamics was reported for an invar-type $Fe_{72}Pd_{28}$.[29] The lattice-dynamical, or phonon, properties of $FePd_3$ have been studied at low temperatures for their own sake.[30]

Of the two parameters that govern diffusion and ordering kinetics, i.e., $E_F$, the vacancy formation enthalpy, and $E_M$, the vacancy migration enthalpy, $E_M$ is generally less known and more difficult to measure for ordered intermetallic compounds. In pure metals and random alloys, it can be deduced, for example, from stage III of resistivity recovery during annealing after low-temperature irradiation,[31] or thorough analysis of residual resistometry along isothermal and isochronal annealing series.[32,33] Those two methods are, however, very sensitive to the microstructure of the samples and to any impurities or defects.

An alternative method of determining $E_M$ is an evaluation from lattice-dynamical properties, i.e., elasticity and phonon dispersion. Flynn[34] proposed a model for estimating the migration enthalpy in metals of cubic structures from elastic constants. Recently, a model relating the migration enthalpy for nearest-neighbor jumps in cubic metals to the phonon density of states (DOS) has been proposed by Schober *et al.*[35] In pure fcc metals, excellent agreement between calculated and measured values of $E_M$ was found, whereas in bcc metals, where the experimental values are less well known, predictions were obtained that show a pronounced chemical group systematic behavior. This method has been used by Randl *et al.*[36] in $Fe_{1-x}Si_x$ and by Kentzinger *et al.*[37] in $Fe_{1-x}Al_x$ alloys to estimate the migration enthalpies. Strictly speaking, this method to determine $E_M$ is only valid for elemental crystals. An extension of the theory to $L1_2$ ordered alloys has been made[38] very recently. Its extension to $L1_0$ ordered alloys has not been done yet.

In this paper, we present the phonon dispersion for various states of order in $CoPt_3$ and FePd. Elastic constants and several thermodynamic quantities related to the phonon density of states are deduced. We use Schober's theory and its extension to $L1_2$ compounds to estimate the effects of temperature and ordering on the migration enthalpy. The properties of $FePd_3$,[30] derived by similar analyses, are comparatively discussed. This paper is organized as follows: in Sec. II, we report the experimental details, the dispersion curves,

the force constants, the phonon densities of states, and related thermodynamic quantities. Section III describes the models used to calculate the migration enthalpy. The migration enthalpies of $CoPt_3$, FePd, and $FePd_3$ are discussed in this section. Conclusions are drawn in Sec. IV.

## II. PHONON PROPERTIES

### A. Samples

#### *1. $CoPt_3$*

The $CoPt_3$ single crystal was a cylinder of 9 mm in diameter and 11 mm in length oriented parallel to [111]. Its composition determined by chemical analysis is 26 $\pm 1$ at. %Co. The crystal has been subjected to a long annealing (1.7 h at 873 K, 24 h at 823 K, 16 days at 773 K, and 53 days at 753 K) to ensure the $L1_2$ long-range order parameter larger than 0.95, following the ordering procedure established by Leroux *et al.*[13,39]

#### *2. FePd*

An alloy ingot was made by arc melting from an appropriate mixture of 99.99% Fe and 99.95% Pd in an argon atmosphere. A single crystal was grown by the Bridgman method. The composition of the sample might have deviated from nominal values by evaporation during the crystal-growth process, by 1% or 2% toward either side of the stoichiometry. Spark erosion technique was used to shape the bar into a 266-$mm^3$ parallelepiped with faces parallel to the {100} crystallographic planes (dimensions $\approx 7\times 7\times 5$ $mm^3$). A heat treatment under a compressive stress of 10 MPa on one of the (001) faces was applied in order to obtain a $L1_0$-ordered single-variant structure.[8] The neutron-diffraction measurement of the fundamental and superstructure peak intensities has shown that the dominant variant, whose $c$ axis is parallel to the direction of the compressive stress, is indeed about 99% in volume.

### B. Inelastic neutron scattering

Inelastic neutron-scattering measurements were performed on the 2T1 3-axis spectrometer near Orphée reactor of the Laboratoire Léon Brillouin. The final wave vector was fixed at $k_f = 2.662$ $Å^{-1}$ and scans were performed either in the constant-$h\nu$ mode or in the constant-$\mathbf{q}$ mode, depending on the slope of the phonon-dispersion curve at the measured $(\mathbf{q},\nu)$ point. (002) pyrolytic graphite monochromator and analyzer were used as well as a filter to suppress higher-order contamination.

The crystal was contained in a furnace with a vacuum of the order of $10^{-4}$ Pa or better at high temperature. The crystal was aligned by tilting the furnace with a two-axis goniometer. The sample temperature was measured with two independent thermocouples placed out of the neutron beam. The nominal temperature was stable within $\pm 2$ K, and its absolute value at high temperature was recalibrated using the experimentally determined order-disorder temperature.

To check the effect of temperature and CLRO on the dispersion curves and the deduced physical parameters, phonon frequencies were measured in a highly ordered state at room temperature for both samples, in a partially ordered state at 930 K for $CoPt_3$ and 860 K for FePd, and in a disordered state at 1060 K for $CoPt_3$ and 1020 K for FePd. For both systems, in the last case, the intensity of a superlattice diffraction peak was followed to ensure the collapse of the ordered structure.

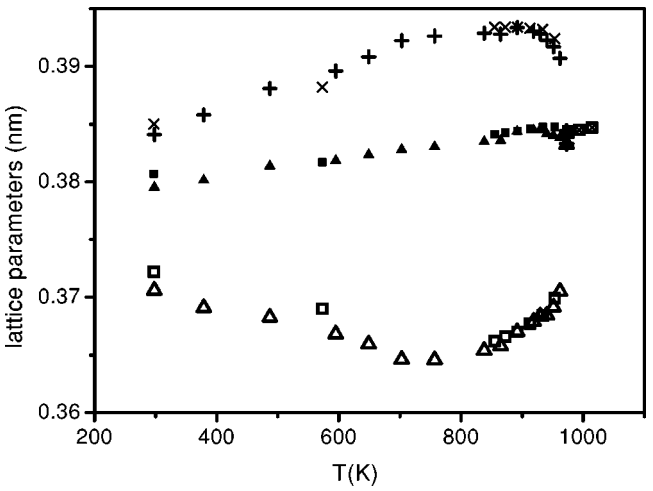


FIG. 3. Lattice parameters of FePd measured by neutron diffraction in the present work are $a$ (+), $c$ (△), $\bar{a}$ (▲), and those measured by x-ray diffraction (Ref. 9) are $a$ (×), $c$ (□), $\bar{a}=(a^2c)^{1/3}$ (■).

### C. Method of analysis

Theoretical dispersion curves have been fitted to the measured phonon frequency spectra $[\nu(\mathbf{q})]$ using the harmonic approximation and the Born–von Karman (BVK) model. This force-constant model assumes that the potential energy of the crystal is a sum of spherical two-body potentials taken over all the pairs of atoms. The interaction between any two atoms at any distance from each other is reduced to two force constants. This reduction to axially symmetrical forces (instead of using a more general tensor model) greatly simplifies the interpretation of the force constants.[40] The appropriate number of neighbor shells is found by trial: the maximum radius of considered neighbors is increased until the fit quality converges.

### D. Order-disorder transition behavior of FePd

First, we report here the order-disorder transition behavior of FePd observed by neutron diffraction during the course of the inelastic-scattering experiment. The state of CLRO of the sample was monitored by measuring the intensities of Bragg peaks. At the same time, the lattice parameters were measured as functions of temperature from the positions of fundamental Bragg peaks. In practice, the positions and the intensities of the 002 and 110 peaks (notations referring to the face-centered cell) were followed between 300 K and 1020 K. However, because of an inadequate experiment setup, the absolute values of the lattice parameters turned out inaccurate; they have been rescaled to the data from another

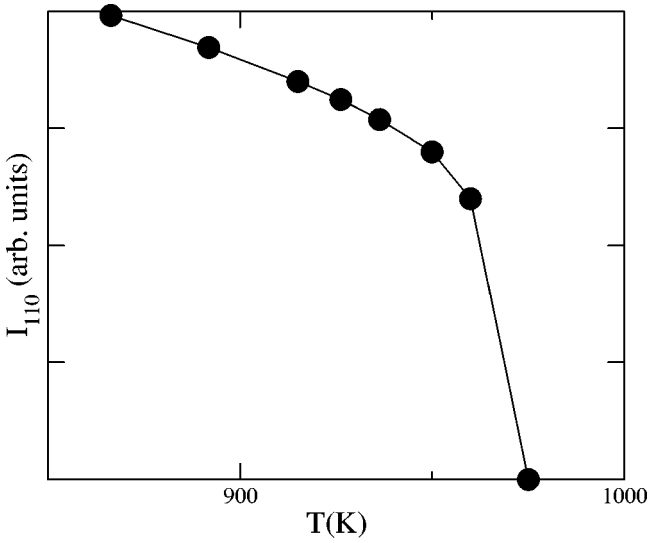


FIG. 4. The intensity of the 110 superlattice Bragg peak from FePd measured by neutron diffraction.

source,[9] but relative variations are significant. Figure 3 shows the temperature dependence of the lattice parameters *a* and *c* (referred to the face-centered cell) and the ''average'' lattice parameter $\bar{a}$, characteristic of the atomic volume.

With increasing temperature, below 800 K, *a* increases but *c* decreases, both almost linearly with temperature (Fig. 3). Eventually, at temperatures above 800 K the trends change and the two parameters converge to the *a* parameter of the disordered fcc structure around 950 K. In the whole range of temperature, the average parameter $\bar{a}$ increases steadily and linearly with temperature, with a slight decrease at the order-disorder transition. These observations are in good agreement with those of Tanaka and Morioka.[9]

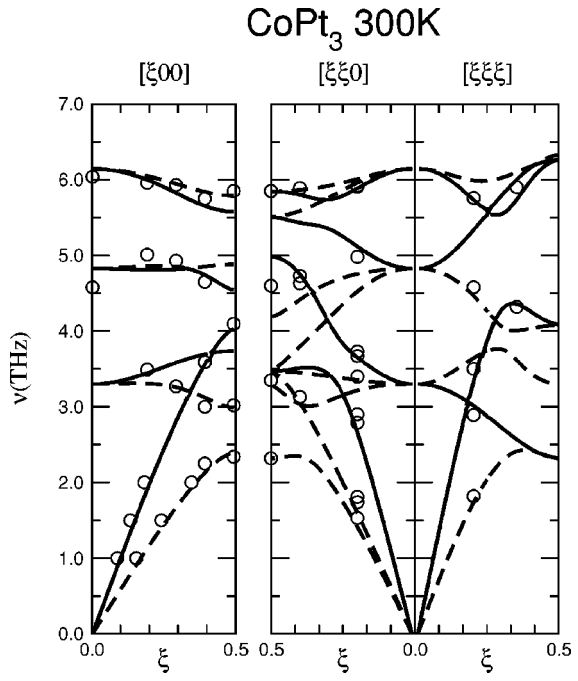


FIG. 5. Phonon dispersion in $L1_2$ ordered $CoPt_3$ at 300 K. Circles show measured phonon frequencies. Solid and dashed curves indicate dispersion curves of longitudinal and transversal branches determined by fitting the BVK model to the experimental data.

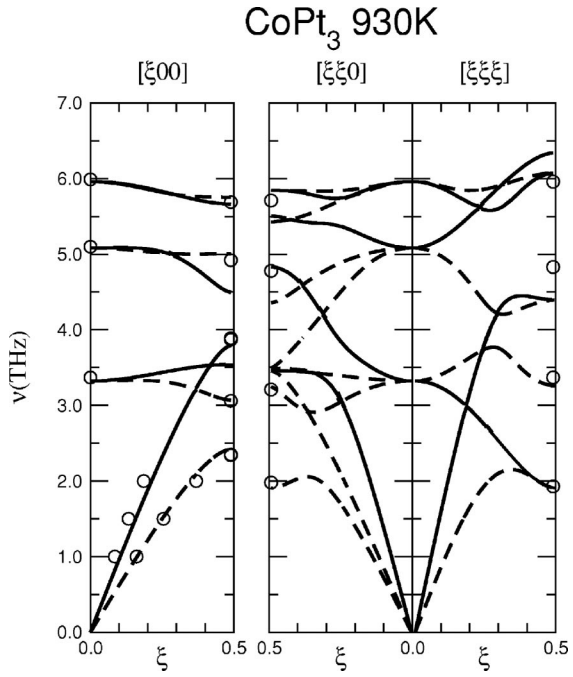


FIG. 6. Phonon dispersion in $L1_2$ ordered $CoPt_3$ at 930 K. The meanings of the symbols are the same as in Fig. 5.

The apparently anomalous decrease of *c* observed below 800 K is interpreted as resulting from the competition between thermal expansion and attractive interaction between Fe and Pd atoms; the distance between neighboring unlike atoms increases with temperature much less than the distance between neighboring like atoms, which manifests itself as the variations of *a* and *c* observed here. In any case, the temperature dependence of the lattice parameters suggests that significant decrease in the CLRO begins at about 800 K.

The chemical disordering has been followed within the neutron spectrometer through the maximum intensity of the 110 superstructure peak (Fig. 4). At each temperature, we did several scans and found that the equilibrium was attained immediately (the annealing due to the peak position optimization lasted only some minutes). The sudden character of the variation of the CLRO and lattice parameters observed through neutron diffraction confirms that the disordering of the $L1_0$ ordered tetragonal structure has short relaxation times. Moreover, the temperature variation of the $L1_0$ structure lattice parameters at the transition is characteristic of the $L1_0$-ordered phase; similar behavior was observed in NiPt, CoPt, and FePt equiatomic alloys.[13,41]

### E. Phonon spectra: Measurement and analysis

Phonon frequencies have been measured along the high-symmetry directions [100], [110], and [111], in the ordered and disordered phases and for the two alloys. In the $L1_0$ phase of FePd, measurements have also been done in [001] and [101], which are not equivalent to [100] and [110]. The

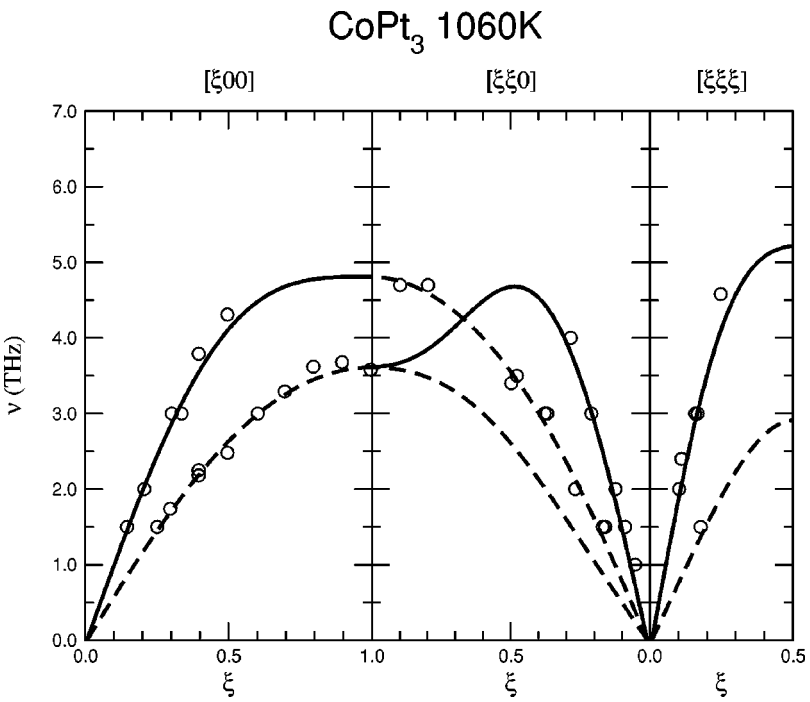


FIG. 7. Phonon dispersion in disordered $CoPt_3$ at 1060 K. The meanings of the symbols are the same as in Fig. 5.

phonon-dispersion curves are reported in Figs. 5–7 for $CoPt_3$, and in Figs. 8–11 for FePd. In all cases, the notations for cubic crystals are used for convenience. The main difference between the ordered (either $L1_2$ or $L1_0$) and disordered states is that new branches (optical modes) appear in the former because of the increase in the number of atoms per elementary unit cell. However, in these systems, the separation between the acoustical and optical branches is not sufficient to create a gap.

### *1. $CoPt_3$*

Figures 5, 6, and 7 show phonon frequency spectra of $CoPt_3$ at 300 K and 930 K in the $L1_2$ ordered state and at 1060 K in the disordered state, respectively. Because of the limited experiment time available, the measured frequencies are not sufficient to delineate all the dispersion curves by themselves, particularly in the measurement at 930 K. Nevertheless, it is possible to draw dispersion curves with the help of the BVK model as shown in the figures, primarily owing to the general properties of phonons in fcc crystals[42] and to the geometry of the measurements. The curves are those obtained by fitting the model to the experimental data taking into account the polarization of the phonon when known. As the unit cell of the $L1_2$ structure contains four atoms, there are 12 phonon branches, three acoustical and nine optical. For the high-remperature measurement, the fitting is done starting with the results at 300 K. In the disordered phase, no optical branches are expected and observed. In the figures, longitudinal and transversal branches are displayed as solid and dashed curves, respectively. The latter are all doubly degenerated in the [100] and [111] directions.

By comparing Figs. 5 and 6, it is evident that the phonon properties at the two temperatures in the ordered state are almost identical: for all measured points, the frequencies are only slightly reduced at 930 K. This indicates that anharmonic effects are not important in this range of temperature. Figure 7 is a typical dispersion spectrum for a fcc metal with an *extremum* of the second acoustical transverse $[\xi\xi 0]$ branch located at $\xi = 0.5$.

The force constants obtained by fitting the BVK model are shown in Table I for the ordered states and in Table II for the disordered state. In the fitting, interactions up to the second-neighbors have been taken into account for the ordered states, with the transversal forces at the second neighbor distance constrained to zero, leading to a set of six adjustable parameters. On the other hand, for the disordered

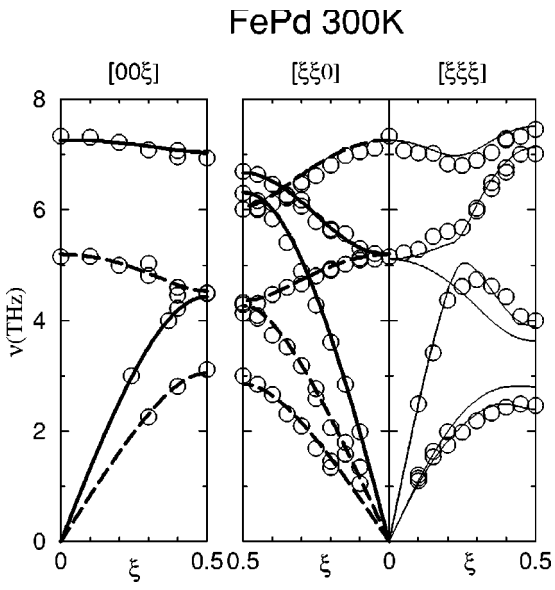


FIG. 8. Phonon dispersion for [001], [110], and [111] directions in $L1_0$ ordered FePd at 300 K. The meanings of the symbols are the same as in Fig. 5, except for the thin solid curves, which indicate branches of mixed polarization.

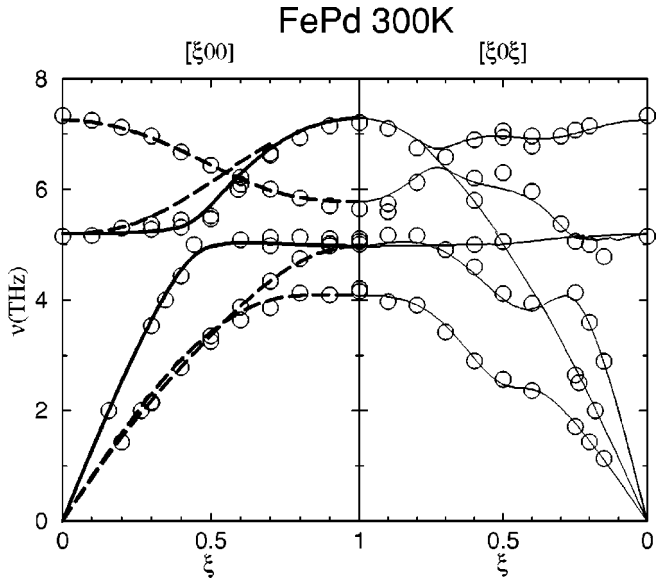


FIG. 9. Phonon dispersion for [100] and [101] directions in $L1_0$ ordered FePd at 300 K. The meanings of the symbols are the same as before.

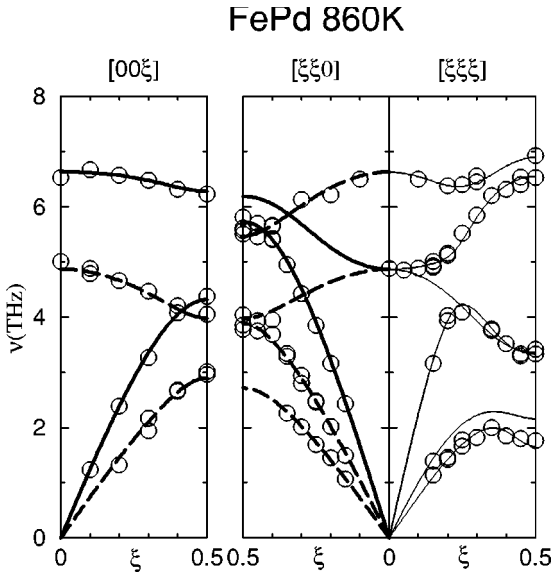


FIG. 10. Phonon dispersion for [001], [110], and [111] directions in $L1_0$ ordered FePd at 860 K. The meanings of the symbols are the same as in Fig. 8.

state, where the fitting has been done with a single species of atoms of the average mass, interactions up to the third neighbors have turned out to be necessary. The transversal force constants $T_n$ are found to be an order of magnitude smaller than the longitudinal ones, $L_n$, in both the ordered and disordered states. The very weak softening observed in the dispersion curves of the two temperatures in the ordered phase is reflected in the small variations in the force constants with temperature (Table I).

#### *2. FePd*

Figures 8–11 show measured phonon frequencies and dispersion curves determined by fitting for $L1_0$ ordered states (Figs. 8 and 9 at 300 K, Fig. 10 at 860 K) and for a disordered state (Fig. 11 at 1020 K). As the elementary tetragonal cell of the $L1_0$ structure involves two atoms per cell (thick line in inset of Fig. 2), six phonon branches, three acoustical and three optical, exist at each **q**. Longitudinal and transversal branches are displayed as thick solid and dashed curves in the same way as for $CoPt_3$. In crystals of the tetragonal structure, however, some of the branches are mixed in character, and those branches are plotted as thin solid curves. In some high-symmetry directions such as [100], [001], and [110], all branches are purely either longitudinal or transversal, and in [001] the transversal branches are doubly degenerated, similar to the case of cubic crystals. No such complications arise in the data at 1020 K (Fig. 11), where the structure is disordered face-centered cubic.

A general trend found from the phonon spectra at the three temperatures is an overall lowering of the frequencies between 300 and 860 K, the effect being much stronger than

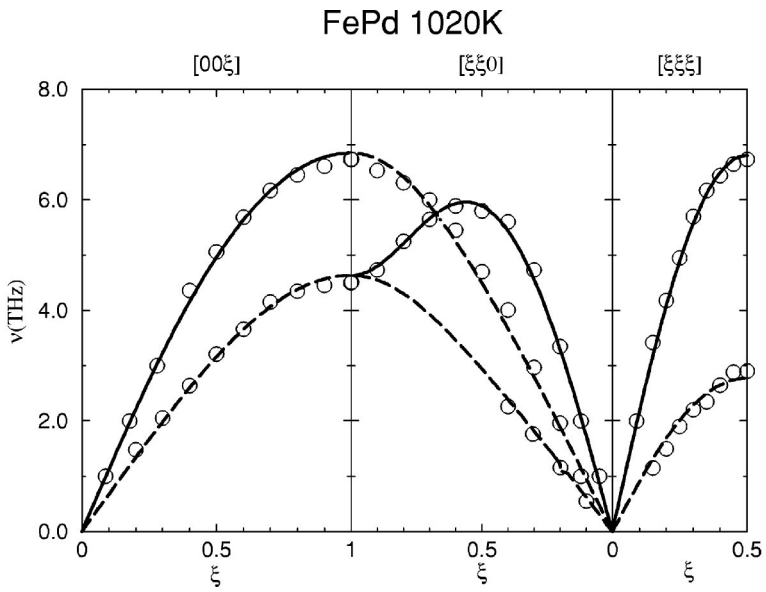


FIG. 11. Phonon dispersion in disordered FePd at 1020 K. The meanings of the symbols are the same as in Fig. 5.

TABLE I. Longitudinal ($L_n$) and transversal ($T_n$) force constants (in N/m) determined by fitting the BVK model to measured phonon frequencies in $L1_2$ ordered $CoPt_3$ (at 300 K and 930 K) and $FePd_3$ (at 80 K). The notation $A$-$B_n$ indicates $A$-$B$ pairs in the $n$th shell of neighbors. $M$ is either Co or Fe and $P$ is either Pt or Pd.

| | | $CoPt_3$ (300 K) | | $CoPt_3$ (930 K) | | $FePd_3$ (80 K) | |
|---|---|---|---|---|---|---|---|
| Pair | Coordinate | $L_n$ | $T_n$ | $L_n$ | $T_n$ | $L_n$ | $T_n$ |
| $P$-$P_1$ | $\frac{1}{2}\frac{1}{2}0$ | 58.7 | −3.6 | 59.9 | −3.0 | 54.2 | −2.3 |
| $M$-$P_1$ | $\frac{1}{2}\frac{1}{2}0$ | 28.1 | 0.8 | 22.0 | 3.4 | 23.6 | −0.8 |
| $P$-$P_2$ | 100 | 9.9 | | 9.9 | | −0.1 | |
| $M$-$M_2$ | 100 | 0.7 | | 4.8 | | 4.6 | |

in $CoPt_3$ between 300 and 930 K. The lowering is particularly significant in the optical branches in $[00\xi]$ and $[\xi\xi0]$, and the acoustical transverse branches in the [111] direction. Some recent x-ray-diffraction results[26] have shown that the CLRO changes significantly between 300 and 860 K. It is thus more difficult to separate in FePd the direct effects of temperature (lattice expansion, anharmonicities, etc.) from the effect due to the CLRO change. Nevertheless, as in fcc transition-metal compounds, the migration enthalpy is generally considered as constant at constant CLRO, we can mainly attribute the phonon changes to the CLRO change.

The force constants obtained by fitting the BVK model are listed in Tables II and III. For the ordered states, the fitting has been done with 21 adjustable parameters, by considering longitudinal interactions up to the fourth nearest neighbors and transversal ones up to the second nearest neighbors (in the fcc notation). The fitting for the fcc disordered state has been made in the same way as for the disordered $CoPt_3$. The softening observed in the phonon frequencies in the ordered phase manifests itself as the decrease with temperature in the predominant force constants, which are the longitudinal force constants between the first-neighbor atoms. The force constants in the disordered state are found to be similar in magnitude to those for the disordered $CoPt_3$.

### F. Phonon densities of states (DOS)

Using the atomic force constants obtained from the BVK fits, the total phonon DOS $Z(\nu)$ has been obtained at each temperature from the dispersion relations $\nu_s(\mathbf{q})$ by integration over the first Brillouin zone:

$$Z(\nu)=\frac{1}{3N}\frac{V}{(2\pi)^3}\sum_s\int\delta(\nu-\nu_s(\mathbf{q}))d\mathbf{q}, \qquad (1)$$

TABLE II. Force constants (in N/m) determined by fitting the BVK model to measured phonon frequencies in disordered $CoPt_3$ (at 1060 K) and FePd (at 1020 K). The numbers in parentheses indicate possible errors in the last digit.

| | | $CoPt_3$ | | FePd | |
|---|---|---|---|---|---|
| $n$ | Coordinate | $L_n$ | $T_n$ | $L_n$ | $T_n$ |
| 1 | $\frac{1}{2}\frac{1}{2}0$ | 33.0(6) | −3.0(2) | 32.4(4) | −2.1(2) |
| 2 | 100 | 4.7(5) | 0.8(2) | −0.1(3) | −0.9(2) |
| 3 | $\frac{1}{2}\frac{1}{2}1$ | 4.1(5) | 0.9(3) | 0.8(1) | 0.0(1) |

where $V$ is the volume of the unit cell and $N$ is the number of atoms per unit cell. The sum runs over all phonon branches $s$. The integration is carried out numerically by scanning the Brillouin zone by the method first proposed by Gilat and Raubenheimer.[43]

Another interesting quantity is the so-called partial phonon DOS for the atom λ:

$$Z_\lambda(\nu)=\frac{1}{3N}\frac{V}{(2\pi)^3}\sum_s\int|\mathbf{e}_\lambda^s(\mathbf{q})|^2\delta(\nu-\nu_s(\mathbf{q}))d\mathbf{q}, \qquad (2)$$

where $\mathbf{e}_\lambda^s(\mathbf{q})$ is the normalized eigenvector at the wave vector $\mathbf{q}$ of the dynamical matrix for atom λ and for the phonon branch $s$. The sum of the partial densities of states over λ gives the total DOS.

#### 1. $CoPt_3$

As expected from the phonon-dispersion curves, the DOS constitutes a continuous spectrum at all the three temperatures (Fig. 12). The shift in the total DOS between 300 K and 930 K is very small, reflecting the weak softening in the $L1_2$ ordered phase (which was directly visible in the dispersion curves). The low-frequency part of the DOS in the ordered phase consists mostly of the contribution of the heavier species (Pt, dashed curve), while the contribution of the lighter species (Co, dotted curve) appears only at the uppermost frequency range above 5.4 THz. The DOS in the disordered state (at 960 K) shows features typical of elemental fcc crystals, consisting of contributions of the two transversal modes from low to intermediate frequencies and that of the longitudinal mode at high frequencies.

#### 2. FePd

The calculated phonon DOS of FePd at the three experiment temperatures are shown in Fig. 13. As in $CoPt_3$, the DOS spectrum is continuous. In contrast to the case of $CoPt_3$, however, the softening of the lattice with increasing temperature in the ordered phase is apparent as a shift of the whole spectrum toward lower frequencies: the cutoff frequency is 7.5 THz at 300 K but is lowered to 6.9 THz at 860 K. In $CoPt_3$ the contribution of the heavier species to the total DOS is dominant at low frequencies and that of the lighter species is important at high frequencies. In FePd, the same trend is still noticeable but is much weaker, probably because of the far smaller difference in mass between the

TABLE III. Longitudinal ($L_n$) and transversal ($T_n$) force constants (in N/m) determined by fitting the BVK model to measured phonon frequencies in $L1_0$ ordered FePd (at 300 K and 860 K). The neighbors are indexed referring to the fcc structure. The notation $A$-$B_{nZ}$ indicates the $n$th neighbor $A$-$B$ pairs with $Z$ orientation [$Z=x$ (equivalent to $y$) or $z$].

| | | 300 K | | 860 K | |
|---|---|---|---|---|---|
| Neighbor | Coordinate | $L_n$ | $T_n$ | $L_n$ | $T_n$ |
| Pd-$Pd_1$ | $\frac{1}{2}\frac{1}{2}0$ | 52.1(9) | −2.7(6) | 41.8(9) | −2.9(7) |
| Fe-$Pd_1$ | $\frac{1}{2}0\frac{1}{2}$ | 34.3(4) | −2.1(3) | 30.6(6) | −2.5(5) |
| Fe-$Fe_1$ | $\frac{1}{2}\frac{1}{2}0$ | 21.3(9) | −1.6(6) | 15.4(9) | −4.1(9) |
| Pd-$Pd_{2z}$ | 001 | 0.2(9) | −0.5(6) | 2.9(7) | −1.8(2) |
| Fe-$Fe_{2z}$ | 001 | 3.4(9) | −2.4(3) | 2.2(9) | −2.9(6) |
| Pd-$Pd_{2x}$ | 100 | −0.1(9) | 0.9(5) | −0.4(9) | −0.4(1) |
| Fe-$Fe_{2x}$ | 100 | 1.2(6) | −2.8(5) | 2.4(9) | −0.3(1) |
| Fe-$Fe_3$ | $\frac{1}{2}\frac{1}{2}1$ | 0.8(5) | 0.0 | 1.4(9) | 0.0 |
| Pd-$Pd_3$ | $\frac{1}{2}\frac{1}{2}1$ | 1.1(6) | 0.0 | −0.5(3) | 0.0 |
| Fe-$Pd_3$ | $\frac{1}{2}1\frac{1}{2}$ | 0.9(3) | 0.0 | 0.9(4) | 0.0 |
| Fe-$Fe_{4z}$ | 202 | 4.3(5) | 0.0 | 2.0(9) | 0.0 |
| Pd-$Pd_{4z}$ | 202 | −0.2(6) | 0.0 | 2.4(2) | 0.0 |
| Fe-$Fe_{4x}$ | 220 | −2.9(6) | 0.0 | −0.6(9) | 0.0 |
| Pd-$Pd_{4x}$ | 220 | 3.8(9) | 0.0 | −2.7(9) | 0.0 |

two constituent species; the contributions of the two species of atoms are distributed more or less similarly, particularly at 300 K. The DOS in the disordered state is again typical of elemental fcc crystals.

Here, it is interesting to note that the lowering of the cutoff frequency is appreciable between temperatures encompassing the order-disorder transition in $CoPt_3$, while it occurs in the ordered phase in FePd. This can be attributed to the constant CLRO up to the order-disorder transition in $CoPt_3$, whereas the CLRO is suggested to change significantly in the range well below this temperature in FePd.[26]

### G. Comparison with $FePd_3$

Phonon-dispersion spectra of $L1_2$ ordered $FePd_3$, which is isomorphous to $CoPt_3$ and consists of the same elements as FePd, were measured by inelastic neutron scattering at 80

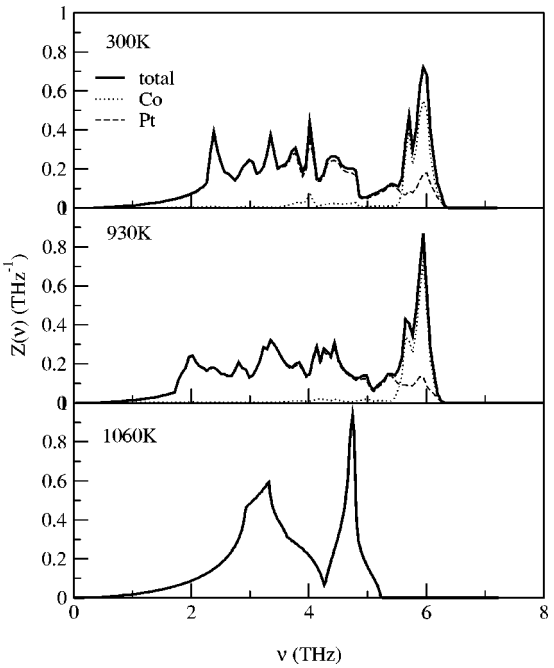


FIG. 12. Phonon DOS of $CoPt_3$ in $L1_2$ ordered states (300 K and 930 K) and in disordered state (1060 K). Dotted and dashed curves in the upper two figures denote partial DOS of Co and Pt, respectively.

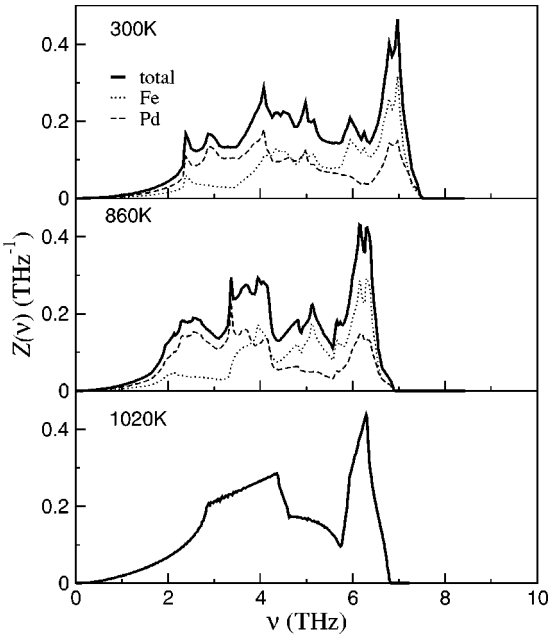


FIG. 13. Phonon DOS of FePd in $L1_0$ ordered states (300 K and 860 K) and in disordered state (1020 K). Dotted and dashed curves in the upper two figures denote partial DOS of Fe and Pd, respectively.

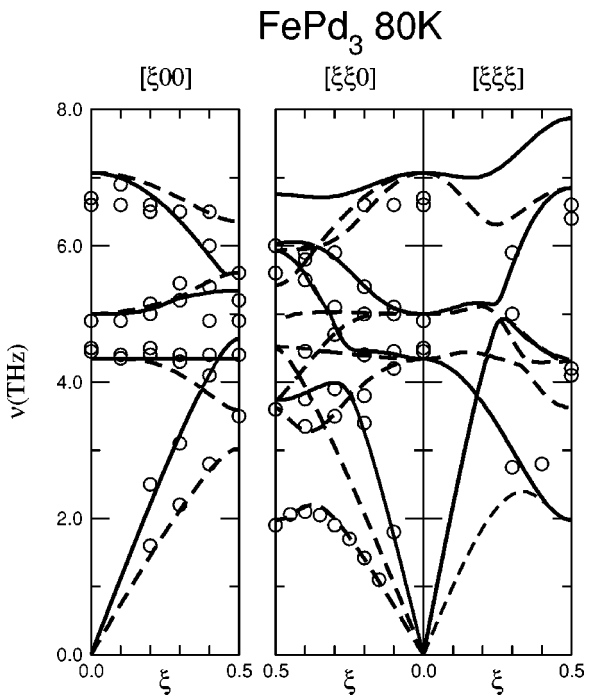


FIG. 14. Phonon dispersion in $L1_2$ ordered $FePd_3$ at 80 K (Ref. 30). The meanings of the symbols are the same as in Fig. 5.

K by Stirling *et al.*[30] We have analyzed their data by the same method employed for $CoPt_3$ to compare the properties of phonons with those in $CoPt_3$ and FePd.

Figure 14 shows the phonon frequencies reported by Stirling et al. and the dispersion curves determined using the BVK model. The fitting has been made with the same conditions as $CoPt_3$ with six adjustable parameters. Some features of the phonon properties of $FePd_3$ are found to be common to the $L1_0$ ordered FePd (Figs. 8–10): the maximum frequencies are about 7 THz in both cases, the sound velocities in equivalent directions (i.e., the slopes at the center of the Brillouin zone) are almost equal. In the [111] direction the anticrossing between the longitudinal acoustic and optic branches appears in both materials at $\xi=0.3$, but the gap in $FePd_3$ is much smaller.

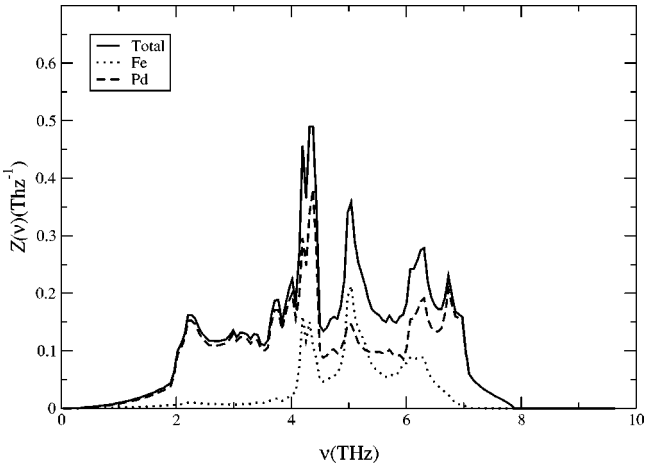


FIG. 15. Partial and total phonon DOS of $L1_2$ ordered $FePd_3$ at 80 K.

TABLE IV. Elastic constants (in GPa) obtained from the slope of the phonon-dispersion curves and those determined by ultrasonic measurements (Ref. 45) (noted FePd*). Errors are estimated to be ±5 GPa.

| Alloy ($T$) | $C_{11}$ | $C_{12}$ | $C_{33}$ | $C_{44}$ | $C_{66}$ |
|---|---|---|---|---|---|
| $CoPt_3$ (300 K) | 297 | 130 | | 102 | |
| (1060 K) | 308 | 227 | | 103 | |
| $FePd_3$ (80 K) | 206 | 122 | | 90 | |
| FePd (300 K) | 248 | 159 | 239 | 95 | 86 |
| (860 K) | 202 | 122 | 200 | 76 | 48 |
| (1020 K) | 178 | 125 | | 64 | |
| FePd* (1020 K) | 159 | 117 | | 64 | |

The force constants determined by the analysis are listed in Table I. They are similar to those of the ordered $CoPt_3$ (in the same table), in that the longitudinal force constants between the first-neighbor atoms, particularly between the heavier species of atoms, are far more important than the others. At the same time, inspection of Table III shows that the corresponding force constants of $L1_0$ ordered FePd to those of $FePd_3$ are also close to each other. Nevertheless, a notable difference exists among the three alloys in the interaction between the second-neighbor atoms: the force constant is larger between Fe atoms in $FePd_3$ and FePd, whereas that between Pt atoms is dominant in $CoPt_3$.

The partial and total phonon DOS of $FePd_3$ are shown in Fig. 15. The overall shape of the spectrum is to some extent similar to that for $L1_0$ ordered FePd (Fig. 13) at 300 K, except that the peaks at intermediate frequencies are larger than those at high frequencies. The contribution of Fe atoms is rather confined at three frequency ranges to form well-defined peaks, while that of Pd atoms are widely spread. This character may be regarded as intermediate between $CoPt_3$ and FePd, where the partial DOS of the two species of atoms appear at distinct frequency ranges ($CoPt_3$) and at almost all frequencies (FePd), respectively. Understanding these features, together with the subtle differences in the force constants, may require detailed theoretical analysis, such as the one made for various intermetallics and oxides by Parlinski *et al.*[44]

### H. Calculation of elastic constants

The elastic constants of $CoPt_3$, FePd, and $FePd_3$ have been calculated using the relations between the sound velocities and elastic constants for tetragonal crystals given by Cummins *et al.*[42] The sound velocities have been deduced from the slopes of the high-symmetry phonon branches at the center of the Brillouin zone. The results are given in Table IV.

Ichitsubo[45] measured the elastic constants of disordered FePd by ultrasonic resonance spectrometry at temperatures below 320 K (using a quenched sample) and above 920 K. The values of the present work in FePd at 1020 K are in fair agreement with his results.

TABLE V. Thermodynamic properties calculated in the harmonic approximation from the density of states for the different temperatures. $S_V$ refers to the average vibrational entropy per atom, $\theta_D$ to the Debye temperature, $C_V(T)$ to the specific heat per atom, and $C_V(300\ \mathrm{K})$ to the specific heat per atom at 300 K extrapolated using the Debye approximation. $k_B$ is the Boltzmann constant. The last two columns show the migration enthalpies (in eV), deduced from Flynn's model ($E_M^{Fly}$) in the fcc disordered state and deduced from Schober's model ($E_M^{av}$) assuming a fcc lattice with an atomic mass equal to the averaged mass of the compound.

| Alloy | $T$(K) | $S_V/k_B$ | $\theta_D$ (K) | $C_V(T)/k_B$ | $C_V$ (300 K)$/k_B$ | $E_M^{Fly}$ | $E_M^{av}$ |
|---|---|---|---|---|---|---|---|
| $CoPt_3$ | 300 | 2.24 | 273.6 | 2.87 | 2.87 | | 1.36 |
| | 930 | 2.63 | 272.8 | 2.98 | 2.87 | | 1.33 |
| | 1060 | 2.70 | 228.4 | 2.99 | 2.91 | 0.95 | 1.13 |
| $FePd_3$ | 80 | 2.15 | 297 | 1.63 | 2.83 | | 0.94 |
| FePd | 300 | 2.15 | 318.7 | 2.82 | 2.82 | | 0.91 |
| | 860 | 2.64 | 284.3 | 2.97 | 2.86 | | 0.66 |
| | 1020 | 2.66 | 286.8 | 2.98 | 2.86 | 0.78 | 0.74 |

### I. Calculation of related thermodynamic quantities

From the phonon DOS, we have calculated the Debye temperature, the average vibration entropy per atom, and the specific heat per atom within the harmonic approximation.[46,47] These values are given in Table V. The specific heat has been extrapolated to room temperature, assuming a variation obeying the Debye law,[47] to allow a comparison between the three alloys.

The Debye temperature appears relatively sensitive to the state of order: a decrease of 10–15 % is observed between the ordered and the disordered states. As expected, the vibration entropy per atom increases significantly (25%) with temperature. The gain in the vibrational entropy ($\Delta S_V$) at the order-disorder transition can be estimated to $0.51k_B$ and $0.46k_B$, respectively, for FePd and $CoPt_3$. These large vibrational entropy differences can be due either to a change in the character of the vibrational spectrum associated with the chemical disordering of the systems or to the difference in the phase-space volume between the ordered and the disordered phases. The values of the specific heat extrapolated at 300 K are very close to each other. The effect of the ordering is visible but small; in the disordered state $C_V(300\ \mathrm{K})$ is higher than in the ordered state systematically but only by $0.04k_B$.

The comparison of those values confirms the difference in behavior of FePd and $CoPt_3$: the main changes take place between 300 K and $T_C-50$ K in the first case and between $T_C-50$ K and $T_C+50$ K in the latter. All the physical quantities related to the phonon spectra exhibit the same behavior, changing correlatively to the CLRO. At high temperatures, the value of the specific heat of $CoPt_3$ and FePd approaches $3k_B$ following the Dulong-Petit law.

TABLE VI. Static lattice Green functions of $CoPt_3$ and $FePd_3$ in the $L1_2$ phase (in $10^{-2}$ m/N) and migration enthalpies (in eV) deduced from the model developed by Kentzinger *et al.* (Ref. 38). *A* refers to the majority atoms (Pt or Pd) and *B* to the minority ones (Co or Fe).

| Alloy | $T$(K) | $G_{xx}^{AA}$ | $G_{zz}^{AA}$ | $G_{xx}^{BB}$ | $E_M^{A\to V_A}$ | $E_M^{A\to V_B}$ | $E_M^{B\to V_A}$ |
|---|---|---|---|---|---|---|---|
| $CoPt_3$ | 300 | 0.968 | 0.741 | 1.154 | 1.28 | 1.47 | 1.20 |
| $CoPt_3$ | 930 | 1.048 | 0.734 | 1.101 | 1.35 | 1.43 | 1.19 |
| $FePd_3$ | 80 | 1.264 | 0.929 | 1.553 | 0.97 | 1.14 | 0.90 |

## III. MIGRATION ENTHALPY CALCULATIONS

In this section we present successively the models used for the migration enthalpy calculation with improving degree of approximation and their results in the cases they are valid. All the models assume that the total energy is well approximated by a sinusoidal form so that the knowledge of the phonon properties (the bottom of the well) gives information on the saddle point (the top of the ridge) of atomic jump processes. This approximation has been verified to be valid in various fcc metals and compounds by molecular dynamics.[35]

### A. Flynn's model

This model has been developed for monoelemental cubic lattices and assumes that the migration enthalpy is dominated by the contribution of acoustical modes at the center of the Brillouin zone. Its obvious drawback is that the other low-energy phonons (soft modes) are not directly taken into account.

The migration enthalpy derived by Flynn[34] in the continuum limit reads

$$E_M^{Fly} = C\Omega\delta^2. \tag{3}$$

Here,

$$\frac{15}{2C} = \frac{3}{C_{11}} + \frac{2}{C_{11}-C_{12}} + \frac{1}{C_{44}},$$

where $C_{11}, C_{12}$, and $C_{44}$ are the three independent elastic constants of the cubic crystal and $\Omega$ is the atomic volume. $\delta^2$ is a structure dependent constant, which is to be determined by minimizing the deviations between the experimental val-

ues and $E_M^{Fly}$ in different materials of the structure concerned. Schober *et al.*[35] have obtained $\delta^2=0.081$ for the fcc structure.

The values of the migration enthalpy in the fcc disordered states have been calculated using Eq. (5) and are shown in Table VI. In FePd, the value (0.78 eV) compares well to that obtained with the ultrasonic resonance spectrometry[45] (0.67 eV). In $CoPt_3$ the value is significantly higher, 0.95 eV.

### B. Schober's model for fcc crystals

Schober *et al.*[35] have developed a model relating the migration enthalpy to the whole phonon spectrum through the phonon DOS. In this model, the migration enthalpy is derived from the following relation:

$$E_M=4\pi^2a^2\alpha G_0^{-1}, \tag{4}$$

where

$$G_0=\int \frac{Z(\nu)}{M\nu^2}d\nu.$$

In Eq. (4), $E_M$ separates into a structural factor ($a^2\alpha$), common to all fcc, and an electronic factor ($G_0$), which is the static Green function and reflects the electronic particularities. $a$ is the lattice parameter and $\alpha$ a geometrical constant; $\alpha$ has been determined by computer simulation to be equal to 0.0135 in fcc metals.[35]

The underlying assumption of the model is that diffusion takes place via nearest-neighbor jumps and that the potential has a sinusoidal form along the atom trajectory. In fcc metals, it is commonly accepted that self-diffusion is dominated by the simplest vacancy mechanism, namely, $\frac{1}{2}(1,1,0)$ atomic jumps into a nearest-neighbor vacancy.[48–50]

In the fcc solid solutions, the migration enthalpy was calculated using the Schober and the Flynn models. The value of the migration enthalpy in the Schober model ($E_M^{av}$) is most often slightly higher than the value deduced from the Flynn model.[34]

Strictly speaking, formula (4) is valid only for pure cubic metals. As a first approximation, since the model was not yet extended to $L1_0$ phases, we have considered the FePd $L1_0$ structure as a fcc lattice with an atomic mass equal to the averaged mass of the two atoms. In order to compare all the systems, the $L1_2$ phases have also been treated in a first step within this model; the corresponding migration enthalpies are noted $E_M^{av}$ in Table V.

### C. Extension of Schober's model to $L1_2$ structure

Recently, Schober's model was extended to $A_3B$ compounds with $L1_2$ structure by one of the present authors using the static lattice Green functions of the two constituent species.[38] The Green-function matrix elements $G_{ij}^{mm}$ ($i,j=x,y$ or $z$) of a given atom $m$ can be expressed in terms of the eigenvalues $\nu_s(\mathbf{q})$ and eigenvectors (i.e., polarization vectors) $\mathbf{e}_s(\mathbf{q})$ ($s=1,\ldots,3N$, where $N$ is the number of atoms in the unit cell) of the dynamical matrix at wave vector $\mathbf{q}$ which are known from Born–von Karman fits of the measured phonon-dispersion curves:

$$G_{ij}^{mm}=\int \frac{Z_{ij}^{mm}(\nu)}{M^m\nu^2}d\nu. \tag{5}$$

Here $M^m$ is the mass of atom $m$ and $Z_{ij}^{mm}(\nu)$ is the partial density of states:

$$Z_{ij}^{mm}(\nu)=\frac{1}{3N}\frac{V}{(2\pi)^3}\sum_s \int e_i^{m,s}(\mathbf{q})e_j^{m,s}(\mathbf{q})\,\delta(\nu-\nu_s(\mathbf{q}))d\mathbf{q}, \tag{6}$$

where $V$ is the volume of the unit cell and the integration extends over the first Brillouin zone.

In the case of elemental fcc or bcc metals, the static lattice Green-function matrix of an atom $m$ ($\mathbf{G}^{mm}$) is diagonal and reduces to a single number ($G_0$). In $A_3B$ compounds with the $L1_2$ structure, the positions for $B$ atoms have the cubic point symmetry and the Green-function matrix $\mathbf{G}^{BB}$ also reduces to a single number $G_{xx}^{BB}$. On the other hand, the point symmetry of the positions for the $A$ atoms is tetragonal. For the $A$ atom at position $(\frac{1}{2},\frac{1}{2},0)$ in the unit cell, $\mathbf{G}^{AA}$ is diagonal with $G_{xx}^{AA}=G_{yy}^{AA}\neq G_{zz}^{AA}$. In this case, in a fully ordered lattice with one vacancy, three types of nearest-neighbor jumps are to be considered: the jump of an $A$ atom in an $A$ vacancy ($A\rightarrow V_A$), the jump of an $A$ atom in a $B$ vacancy ($A\rightarrow V_B$), and the jump of a $B$ atom in an $A$ vacancy ($B\rightarrow V_A$).

The Green matrix elements of $L1_2$ ordered $CoPt_3$ and $FePd_3$ have been calculated from the phonon spectra, via the densities of states using the force constants obtained in the BVK fits. The Green functions and the deduced migration enthalpies for each atomic jump and at the different temperatures are compiled in Table VI.

TABLE VII. Correlation of the migration energy to the average atomic mass.

| | $E_M^{av}$(eV) | Average mass (amu) |
|---|---|---|
| FePd | 0.74 | 81 |
| $FePd_3$ | 0.94 | 94 |
| $CoPt_3$ | 1.13 | 161 |

### D. Discussion

The average migration enthalpies calculated for the three systems, $CoPt_3$, FePd, and $FePd_3$, show a tendency to increase with the average atomic mass of the system (Table VII).

The migration energies in the $L1_2$ ordered alloys also show, as expected, an increase with the size of the atom involved in the jump. Moreover, in each alloy, $A\rightarrow V_B$ is associated with the highest $E_M$ and $B\rightarrow V_A$ with the lowest (Table VI).

The migration enthalpy at room temperature in FePd (0.91 eV) is close to the migration barriers obtained by

Kentzinger *et al.*[38] in $FePd_3$ (0.97 eV for a Pd atom migrating within its own lattice and 1.14 eV when it jumps on the Fe lattice; 0.90 eV for an Fe atom leaving its own lattice). With an average atomic mass and the total DOS, we obtain 0.94 eV, very comparable to the value obtained within the same approximation in FePd. In contrast, in $CoPt_3$, the migration enthalpy deduced by the same method is much larger, 1.36 eV, as expected from the effect of atomic mass and size.

The migration enthalpy is expected to decrease with increasing temperature as a consequence of increasing anharmonicity. In fact, Schober's model assumes that the diffusion jump—the most anharmonic conceivable event—follows a trajectory parallel to the direction of low-harmonic-restoring forces. In other words, in the directions where the harmonic part of the potential is low, we expect the anharmonic part, i.e., the migration barrier, to be low as well.

In $CoPt_3$ the effect of temperature is negligible compared with the effect of CLRO: increasing the temperature by 600 K has a very small effect ($-0.03$ eV: within the error bar) compared to disordering the $L1_2$ phase ($-0.20$ eV). In FePd, the concomitant change of CLRO and temperature within the ordered phase makes the comparison difficult.

In intermetallic alloys the activation energy of atomic migration is known to depend on the magnetic state. The Curie temperature of $CoPt_3$ is at room temperature (288 K) whereas in FePd it is as high as 763 K. The difference in behavior of the migration energy between the two systems can thus also be related to the fact that $CoPt_3$ is paramagnetic at all measurement temperatures whereas it is the case for FePd only at 300 K in the three temperatures. As both chemical and magnetic changes of order are coupled due to the mixed terms in the Hamiltonian,[51,52] they must have simultaneously an effect on the vacancy migration.

Recently, Kozubski *et al.*[27] have obtained 0.7 eV as the average migration enthalpy in the ordered paramagnetic phase of FePd, using residual resistivity measurements, in good agreement with our values deduced from neutron measurements in the same chemical and magnetic order state.

Using a Monte Carlo model, based on a nearest-neighbor vacancy jump mechanism and on an Ising Hamiltonian with effective pair interaction energies for first and second neighbors in $L1_2$ and $L1_0$ (Ref. 53) compounds, the contribution of the ordering energy to the mean migration enthalpy have been found equal to $\Delta E_M^{av}/T_C = 0.28$ meV/K and 0.19 meV/K, respectively. $\Delta E_M^{av}$ is the difference between the migration enthalpy in the ordered and in the disordered phases and $T_C$ is the order-disorder transition temperature. The migration enthalpy is larger in the ordered state because, at least in some directions, the migration of the vacancies is accompanied by a change of CLRO that costs some additional energy. It is always the case when the vacancy changes sublattice, contrary to the case where the vacancy remains within one sublattice (the majority atom's sublattice in $L1_2$ and both planar sublattices in $L1_0$).[54] These values are close to $\Delta E_M^{av}/T_C = 0.23$ meV/K and 0.18 meV/K, respectively, obtained experimentally from the present phonon measurements via the Schober model considering the total phonon DOS and an average atom.

## IV. CONCLUSION

Phonon-dispersion curves in $CoPt_3$ and FePd alloys have been measured at 300 K and below the order-disorder transition in the $L1_2$ ordered structure for $CoPt_3$ and in the $L1_0$ ordered phase for FePd. The fcc disordered states have also been investigated above the order-disorder temperature. Comparison is made with the $FePd_3$ system analyzing phonon data measured at 80 K.

A general decrease in phonon frequencies with increasing temperature has been found in FePd. An important shift with temperature has been observed for the acoustical transverse branches in the [111] direction. Those modes appear at a particularly low energy, indicating low potential barriers for atomic displacements. Elastic constants have been calculated in both systems from the slope of relevant phonon-dispersion curves.

From a BVK fit of the measured points, we have calculated the phonon densities of states and estimated the migration enthalpies in FePd using the model proposed by Schober *et al.*[35] and in $CoPt_3$ using its extension to $A_3B$ compounds developed by Kentzinger and Schober.[38] The phonon DOS have also been used to calculate related thermodynamic quantities, namely, the vibrational entropy per atom $S_V$, the Debye temperature $\theta_D$, and the specific heat $C_V$.

The contribution of ordering to the mean migration enthalpies in $CoPt_3$ (0.23 meV/K) and in FePd (0.18 meV/K) obtained experimentally in the present work compare very well with those obtained by Monte Carlo simulation in $L1_2$ and $L1_0$ compounds.

## ACKNOWLEDGMENTS

This work was partly supported by Algerian project ANDRU/PNR3 (Grant No. AU49902) and by a collaborative program 99 MDU 449 between the University Louis Pasteur of Strasbourg, France and the University Mouloud Mammeri of Tizi-Ouzou, Algeria. We thank K. Morioka for his help in preparing the FePd crystal.

*Present address: Physikdepartment E13/FRMII, Technische Universität München, 85747 Garching, Germany.

[1] F. Menzinger and A. Paoletti, Phys. Rev. **143**, 365 (1966).

[2] G.E. Bacon and E.W. Mason, Proc. R. Soc. London **88**, 929 (1966).

[3] G.E. Bacon and J. Crangle, Proc. R. Soc. London **272**, 387 (1963).

[4] M.C. Cadeville and J.L. Moran-Lopez, Phys. Rep. **153**, 331 (1987).

[5] T.H. Kim, M.C. Cadeville, A. Dinia, and H. Rakoto, Phys. Rev. B **53**, 221 (1996); T.H. Kim, M.C. Cadeville, A. Dinia, V. Pierron-Bohnes, and H. Rakoto, *ibid.* **54**, 3408 (1996).

[6] S. Zyade, F. Garin, and G. Maire, New J. Chem. **11**, 429 (1987).

[7] M. Morinaga, J. Saito, N. Yukawa, and H. Adachi, Acta Metall.

Mater. **38**, 25 (1990).
[8] K. Tanaka, T. Ichitsubo, and M. Koiwa, Mater. Sci. Eng., A **312**, 118 (2001); K. Morioka and K. Tanaka, in *Proceedings of the Fourth Pacific Rim International Conference on Advanced Materials and Processing (PRICM4)*, edited by S. Hanada, Z. Zhong, S. W. Nam, and R. N. Wright (Japan Institute of Metals, Sendai, 2001).
[9] K. Tanaka and K. Morioka, Philos. Mag. A **83**, 1797 (2003).
[10] G.R. Harp, D. Weller, T.A. Rabedeau, R.F.C. Farrow, and M.F. Toney, Phys. Rev. Lett. **71**, 2493 (1993); A. Cebollada, D. Weller, J. Sticht, G.R. Harp, R.F.C. Farrow, R.F. Marks, R. Savoy, and J.C. Scott, Phys. Rev. B **50**, 3419 (1994).
[11] D. Weller, H. Brändle, and C. Chappert, J. Magn. Magn. Mater. **121**, 461 (1993).
[12] O. Ersen, V. Parasote, V. Pierron-Bohnes, M.C. Cadeville, and C. Ulhaq-Bouillet, J. Appl. Phys. **93**, 2987 (2003).
[13] C. Leroux, M.C. Cadeville, V. Pierron-Bohnes, G. Inden, and F. Hinz, J. Phys. F: Met. Phys. **18**, 2033 (1988).
[14] A.Ye. Yermakov and V.V. Maykov, Phys. Met. Metallogr. **69**, 198 (1990).
[15] S. Shimizu and E. Hashimoto, J. Jpn. Inst. Met. **35**, 902 (1971).
[16] J.M. Sanchez, J.L. Moran-Lopez, C. Leroux, and M.C. Cadeville, J. Phys. C **21**, L1091 (1988); J. Phys.: Condens. Matter **1**, 491 (1988).
[17] M.J. Capitan, S. Lefebvre, Y. Calvayrac, M. Bessière, and P. Cénédèse, J. Appl. Crystallogr. **32**, 1039 (1999).
[18] E. Kentzinger, V. Parasote, V. Pierron-Bohnes, J.F. Lami, M.C. Cadeville, J.M. Sanchez, R. Caudron, and B. Beuneu, Phys. Rev. B **61**, 14 975 (2000).
[19] H. Berg and J.B. Cohen, Metall. Trans. **3**, 1797 (1972).
[20] L. Bouzidi, M. C. Cadeville, and V. Pierron-Bohnes, in *Solid-Solid Phase Transformations in Inorganic Materials*, edited by W. C. Johnson, J. M. Howe, D. E. Laughlin, and W. A. Soffa (The Minerals, Metals and Materials Society, Warrendale, PA, 1994), pp. 431–436.
[21] C.E. Dahmani, M.C. Cadeville, and V. Pierron-Bohnes, Acta Metall. **3**, 369 (1985).
[22] J. Orehotsky and J.L. Orehotsky, J. Appl. Phys. **61**, 1210 (1987).
[23] V. Gehanno, A. Marty, B. Gilles, and Y. Samson, Phys. Rev. B **55**, 12 552 (1997).
[24] P. Kamp, A. Marty, B. Gilles, R. Hoffmann, S. Marchesini, M. Belakhovsky, C. Boeglin, H.A. Dürr, S.S. Dhesi, G. van der Laan, and A. Rogalev, Phys. Rev. B **59**, 1105 (1999).
[25] O. Kubachewski, *Iron Binary Phase Diagrams* (Springer-Verlag, New York, 1982).
[26] I. Schuster, V. Pierron-Bohnes, and A. Marty (unpublished).
[27] A. Kulovits, W. Püschl, W.A. Soffa, and W. Pfeiler, MRS Symposia Proceedings No. 753 (Material Research Society, Warrendale, PA, 2003), p. BB5.37.1-6.
[28] E. Partyka, D. Kmiec, S. Czekaj, and R. Kozubski, in *Proceedings of the VII Seminar on Diffusion and Thermodynamics of Materials, 2002*, edited by J. Cermak and J. Vrestal (Brno, Czech Republic); R. Kozubski (private communication).
[29] M. Sato, B.H. Grier, S.M. Shapiro, and H. Miyajima, J. Phys. F: Met. Phys. **12**, 2117 (1982).
[30] W.G. Stirling, R.A. Cowley, and M.W. Stringfellow, J. Phys. F: Met. Phys. **2**, 421 (1972).
[31] H. Schultz, in *Atomic Defects in Metals*, Landolt-Börnstein, New Series, Group III, Vol. 25, edited by H. Ullmaier (Springer, Berlin, 1991).
[32] E. Balanzat and J. Hillairet, J. Phys. F: Met. Phys. **11**, 1977 (1981).
[33] A. Schulze and K. Lücke, Acta Metall. **20**, 529 (1972).
[34] C.P. Flynn, Phys. Rev. **171**, 682 (1968).
[35] H.R. Schober, W. Petry, and J. Trampenau, J. Phys.: Condens. Matter **4**, 9321 (1992); **5**, 993 (1992).
[36] O.G. Randl, G. Vogl, W. Petry, V. Hennion, B. Sepiol, and K. Nembach, J. Phys.: Condens. Matter **7**, 5983 (1995); O. G. Randl, Ph.D. dissertation, University of Vienna, 1994.
[37] E. Kentzinger, M.C. Cadeville, V. Pierron-Bohnes, W. Petry, and B. Hennion, J. Phys.: Condens. Matter **8**, 5535 (1996).
[38] E. Kentzinger and H.R. Schober, J. Phys.: Condens. Matter **12**, 8145 (2000).
[39] C. Leroux, A. Loiseau, M.C. Cadeville, and F. Ducastelle, Europhys. Lett. **12**, 155 (1990).
[40] G.W. Lehman, T. Wolfram, and R.E. De Wames, Phys. Rev. **128**, 1593 (1962).
[41] K. Morioka, Master thesis, Graduate School of Engineering, Kyoto University, 2002.
[42] H. Z. Cummins and P. E. Schoen, in *Laser Handbook*, edited by F. T. Arecchi and E. O. Schulz-Dubois (North-Holland, Amsterdam, 1972), Vol. 2, Pt. E, pp. 1029–1075.
[43] G. Gilat and L.J. Raubenheimer, Phys. Rev. **144**, 390 (1966).
[44] K. Parlinski, J. Lazewski, and Y. Kawazoe, J. Phys. Chem. Solids **61**, 87 (2000); K. Parlinski and M. Parlinska-Wojtan, Phys. Rev. B **66**, 064307 (2002).
[45] T. Ichitsubo, Ph.D. thesis, Kyoto University, 2000.
[46] M. A. Krivoglaz, *Theory of X-ray and Thermal Neutron Scattering by Real Crystals* (Plenum Press, New York, 1969).
[47] C. Kittel, *Introduction to Solid State Physics* (Wiley, New York, 1976).
[48] N.L. Peterson, J. Nucl. Mater. **69&70**, 3 (1978).
[49] W. Petry, A. Heiming, C. Herzig, and J. Trampenau, Defect Diffus. Forum **75**, 211 (1991).
[50] G. Vogl, W. Petry, T. Flottmann, and A. Heiming, Phys. Rev. B **39**, 5025 (1989).
[51] V. Pierron-Bohnes, M.C. Cadeville, and F. Gautier, J. Phys. F: Met. Phys. **113**, 1689 (1983); V. Pierron-Bohnes, I. Mirebeau, E. Balanzat, and M.C. Cadeville, *ibid.* **114**, 197 (1984).
[52] M.Z. Dang and D.G. Rancourt, Phys. Rev. B **53**, 2291 (1996).
[53] A. Kerrache, H. Bouzar, M. Zemirli, V. Pierron-Bohnes, M.C. Cadeville, and M.A. Khan, Comput. Mater. Sci. **17**, 324 (2000); in *Proceedings of DIMAT2000*, edited by Y. Limoge and J. L. Bocquet (Scitec, Uetikon-Zürich, 2001), pp. 403–409.
[54] P. Oramus, R. Kozubski, V. Pierron-Bohnes, M.C. Cadeville, and W. Pfeiler, Phys. Rev. B **63**, 174109 (2001); R. Kozubski, P. Oramus, W. Pfeiler, M.C. Cadeville, V. Pierron-Bohnes, and C. Massobrio, Arch. Metall. **46**, 145 (2001).